JOURNAL OF CATALYSIS 31, 13–26 (1973)

Diffusion of Normal Paraffins in Zeolite T

Occurrence of Window Effect

R. L. GORRING

Mobil Research and Development Corporation, Central Research Division, Princeton, New Jersey 08540

Received February 28, 1973; accepted May 15, 1973

Diffusion coefficients have been measured for migration of *n*-paraffins ranging in size from ethane to *n*-tetradecane in potassium T zeolite. Diffusivities were observed to be concentration-independent and closely consistent with the Arrhenius relationship with activation energies as high as 16 kcal/mole. An unexpected phenomenon, termed the window effect, was observed. This consisted of molecules in the *n*-dodecane size range diffusing approximately two orders of magnitude faster than those in the *n*-octane size range. Pre-exponential factors for some molecules possessing permanent dipoles were found to be much lower than for *n*-paraffins of comparable size. A compensation effect was found, pre-exponential factors increasing when activation energies increased.

INTRODUCTION

The advent of shape-selective conversions on zeolites, first demonstrated by Weisz and Frilette (*1*), opened up significant potentials for the engineering design of catalysts on a molecular scale. Further work (*2*) illustrated a variety of molecular shape-discriminating reactions such as: selective cracking of *n*-paraffins from mixtures with isoparaffins, selective linear alcohol dehydration, and olefin hydrogenation. Miale, Chen, and Weisz (*3*) showed that the shape-selective cracking of *n*-hexane over erionite is strongly controlled by intracrystalline diffusion. Molecular engineering of shape-selective catalysts has been reviewed (*4*). In such work the ability of zeolites A, offretite, erionite, and T to admit linear or branched molecules is consistent with the molecular sieving behavior expected from their specific intracrystalline channel structure (*6*).

In a study of the product distribution obtained from cracking long-chain normal paraffins over erionite, Chen, Lucki, and Mower (*5*) observed maxima in products at approximately four and twelve carbon numbers with essentially no product appearing in the C8 range. This unexpected behavior raised the question as to whether it was due to an unusual catalytic phenomenon or due to an anomalous transport effect.

The present study examines diffusion of *n*-paraffins in zeolite T, which is an intergrowth of erionite and offretite. The basic objectives are to determine the magnitude of the diffusivities and the manner in which molecular transport in the intracrystalline channel morphology is influenced by paraffinic chain length.

General theories of transport in zeolites do not exist. Riekert (*7*) and Barrer (*8*) have recently presented reviews of diffusion in zeolites. Riekert (*9, 10*) has presented data on diffusion of small molecules in zeolite T and has presented theoretical analyses of unidirectional, single-file and binary diffusion in zeolites.

Barrer and Kerr (*11*) discuss the geometric factors involved in diffusion in erionite, gmelinite, chabazite and levynite—with special emphasis on crystal anisotropy and diffusion pathways. Migration of *n*-paraffins in erionite and chabazite has been studied by Eberly (*12, 13*) and Barrer and Ibbitson (*14*), who observed diffusivities to continuously decrease with molecular weight for hydrocarbons ligher than *n*-octane.

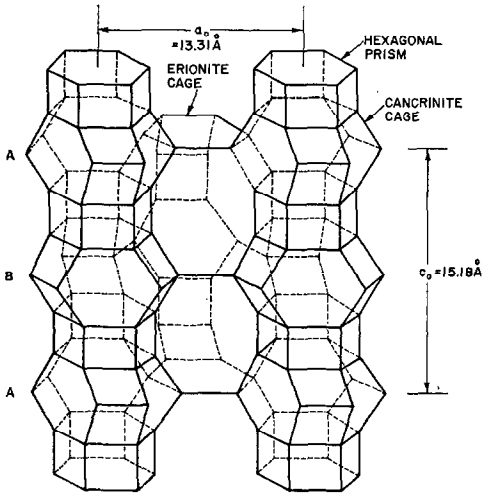

FIG. 1. View of erionite framework.

Structure of Zeolite T—Relation to Diffusion Path

The structure of zeolite T has been determined by Bennett and Gard (*15*) to be composed primarily of offretite with a minor erionite intergrowth. Gard and Tait (*16*) have examined the manner in which the degree of erionite intergrowth can be estimated through odd-l intensities from electron diffraction.

Erionite has a hexagonal lattice structure with two principal crystallographic axes, $\bar{a}$ and $\bar{c}$, as shown in Fig. 1. Figure 1 illustrates the way in which erionite can be constructed from cancrinite cages in a columnar array. These cages, windowed by 6-membered rings, are alternately rotated at 60° to each other giving an ABAB sequence. The internal pore structure accessible to *n*-paraffins is defined by the central cage shown in Fig. 1 and illustrated in Fig. 2(a). The elongated erionite cages approximate the shape of 15.2 × 9.1 Å hexagonal cylinders measuring center-to-center between the aluminum/silicon framework atoms. These are stacked one on top of another and are bound top and bottom by planar 6-membered rings marked A and A′ in Fig. 2(a). Consideration of the ~1.4 Å van der Waals radius of oxygen and measurement with a scale model of erionite shows that the effective mean protrusion of these six-ring oxygen atoms in the $\bar{c}$ direction is ~1.1 A. Thus, the free length of the large cavity is 15.2 − 2(1.1) = 13.0 Å. Similarly, the minimum center-to-center diameter of the 12-ring at the mid-girth pinch in the erionite large cavity is 9.1 Å. Since the oxygen atoms protrude fully around this circumference, the net free diameter of the large cavity is 9.1 − 2(1.4) = 6.3 Å. The large erionite cavity is enclosed by six 8-membered rings (B,C), two planar 6-membered rings (A,A′), three asymmetric 6-membered rings (D) and twelve 4-membered rings (E). The planar 6-membered rings A and A′ in Fig. 2(a) have free diameters of about 2.5 Å and will not permit hydrocarbons to pass from one large cavity to another directly along the $\bar{c}$ direction. The $\bar{a}$ direction in erionite is marked by the arrow (a) in Fig. 2(a) and is defined by 8-membered rings B and C whose planes

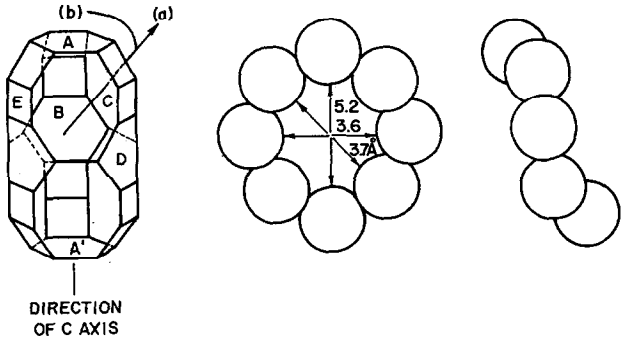

FIG. 2. (a) Erionite cage viewed approximately 20° from direction of $\bar{c}$-axis. (b) Erionite 8-membered ring front and side views. View of offretite framework.

are 60° to each other except for a slight tilt. This 8-membered ring, having a free opening of 3.6 Å, is shown in Fig. 2(b). Thus, the $\bar{a}$ axis is defined by a long column of 8-membered rings which are angled at 30° to its overall direction, slightly tilted, and spaced about 7 Å apart. The free diam of these 8-membered rings normal to the $\bar{a}$ direction is, therefore, approximately 3.6 cos 30° = 3.1 Å.

Figure 3 shows the offretite framework in which the cancrinite units are stacked uniformly one above another in an AAA formation. Also, the basic cage structure (gmelinite cage) is the same width as the large erionite cavity, but is half the height in the $\bar{c}$ direction giving a roughly spherical cage. Thus, the unit cell in offretite is 7.55 Å in the $\bar{c}$ direction. Furthermore, and even more importantly for diffusion, offretite has a continuous, straight, unobstructed large pore of 6.3 Å free diameter running the length of the crystal in the $\bar{c}$ direction. Fault-free offretite should, therefore, be able to sorb cyclic as well as linear molecules. This has recently been demonstrated (*17–19*). The offretite pore is girthed at 7.59 Å intervals by 12-membered ring structures, one of which is shown at the extreme lower part of Fig. 3. The pore conformation in the $\bar{a}$ direction is the same for both offretite and erionite. The $\bar{a}$ direction pore system is more open than the $\bar{c}$ direction pore system in erionite, but less open than the $\bar{c}$ direction large pore system in offretite. Subtle differences in the structures of offretite and erionite are reflected in differences of diffusion within the pores. In erionite, the large hexagonal cavities are the only pathways for molecular migration. Any part of a diffusing molecular must be inside some large erionite cavity. In the case of offretite, the gmelinite cages (see Fig. 3) assume the role of connecting passages between the parallel through-going large pores running the $\bar{c}$ direction.

Zeolite T has been shown (*15, 16, 20*) to be an offretite/erionite intergrowth, with the more open offretite structure being interspersed at intervals with zones of the tighter erionite units. Figure 4 shows the pore geometry of each zeolite in the plane parallel to the $\bar{c}$ axis. In the intergrown zeolite T structure, each occurrence of an erionite cage involves a complete blockage of the large pore (defined by the 12-ring) by a 6-ring as shown in Fig. 4(a). Thus, theoretically, a single unit cell of erionite is sufficient to "dead-end" the large pore of offretite, thus forcing diffusion through 8-rings in the $\bar{a}$ direction and leading to shape-selectivity. A small amount of erionite

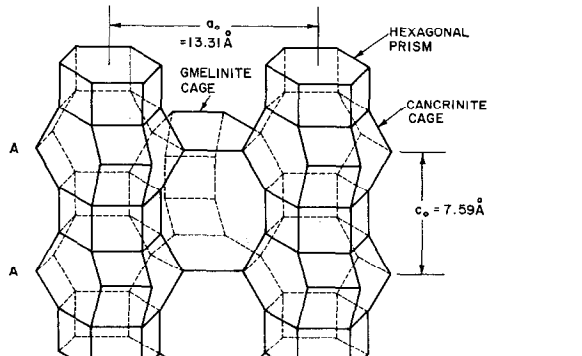

ARRANGEMENT OF SMALL OFFRETITE AND CANCRINITE CAGES IN COLUMNS PARALLEL TO C-AXIS. THE JUNCTION OF THE LINES REPRESENT Si, Al. OXYGEN ATOMS AND CATIONS ARE NOT SHOWN.

FIG. 3. View of offretite framework.

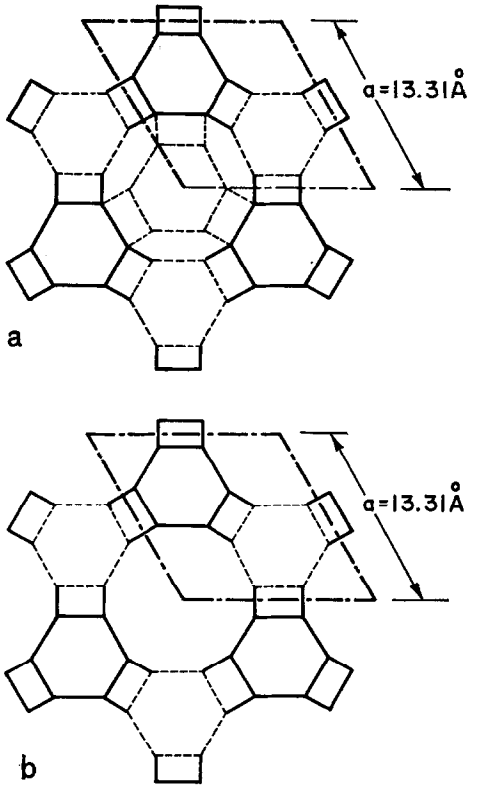

FIG. 4. (a) Projection of erionite framework in plane parallel to $\bar{c}$-axis. (b) Projection of offretite framework in plane parallel to $\bar{c}$-axis.

intergrown in offretite is, therefore, expected to convert offretite, which can sorb large molecules, into a zeolite which can sorb only *n*-paraffins. This has been recently shown by Chen (*6*). Even though erionite constitutes only a portion of the zeolite T structure, these erionite cages are the controlling "bottleneck" factor in diffusion—due to the dead-ending effect referred to above. Therefore, the bulk of the present analysis is concentrated on the relationship of diffusion to the erionite structure.

EXPERIMENTAL

The zeolite T used in this work was made according to the method of Breck and Acara (*21*), and subsequently exchanged with a large excess of potassium ion at room temperature according to methods described by Sherry (*22*). Composition was: potassium 13.9 wt%, sodium 0.07%, silica 69.5%, alumina 16.5%.

X-ray diffraction revealed that the sample contained no significant amorphous material. The faint *l*-odd reflections characteristic of erionite (*15*) indicated that the material was mostly offretite with approximately 2–5% of intergrown erionite. Electron microscope photographs revealed uniform, approximately cylindrical crystals with average length 2.9 μm and diameter 0.65 μm.

n-Paraffins used in this study were Phillips and Humphrey 99.5+% grades which had been thoroughly percolated through silica gel, 5A and 13X molecular sieves to remove any traces of water, olefins, aromatics, and heavy normal paraffins.

Gravimetric analysis was used to determine the rate of diffusion into the zeolite; 5.38 g of zeolite (no binder) were placed in an annular shaped 150 mesh stainless steel basket whose dimensions were: length 3.0 in., o. d. 1.0 in., and i. d. $\frac{7}{8}$ in. The basket was suspended from a quartz rod attached to a copper–bronze spring inside a cylindrical quartz reactor of dimensions $11\frac{3}{4}$ in. $\times$ $1\frac{3}{4}$ in. Temperature was controlled to ± 1°C. Before use, the zeolite sample was heated to 550°C under dry helium for six hours. Experiments were conducted by initially lining out the zeolite at the desired temperature under a flowing stream of dry helium—then establishing a step-function initial condition by replacing the helium flow by a flow of *n*-paraffin. Flow switchover time was about two seconds. All experiments were run at 1 atm total pressure using pure hydrocarbon streams. No measurable sorption of helium was observed under any conditions. Rate of *n*-paraffin diffusion into the zeolite was determined by means of a positional transducer attached to the quartz rod from which the sample basket was suspended. Absolute experimental error was ± 0.03 g hydrocarbon/g zeolite. All sorptions were reversible: the original recorder baseline was attained after stripping with helium. The same 5.38 g of potassium T zeolite was used for all experiments. The sample was stable over a two-month operating period, as deter-

mined by reproduction of experimental diffusivities and by crystallinity measurement.

Raw data output from the experiments consisted of a continuous plot of weight hydrocarbon sorbed into the zeolite vs time from start of run to the establishment of equilibrium. Diffusion coefficients were computed from the theoretical curve using known values of C/C_∞ and time. Diffusion coefficients were computed by comparing the experimental data to the theoretical relationship for radial diffusion into a cylindrical body of constant diffusivity (*23*) using the measured crystallite diameter of 0.65 μm. The radial diffusion model (diffusion assumed predominantly in the crystal $\bar{a}$ direction of zeolite T) was chosen in view of the 2.9 $\times$ 0.65 μm crystal shape and the probably higher diffusivity in the $\bar{a}$ direction for zeolite T.

Shapes of the diffusion curves agreed very closely with the theoretical curve. For propane through *n*-tetradecane, no significant variation of D with concentration was observed up to 80% of equilibrium saturation. Above about 80% saturation, diffusivities declined somewhat with loading. This was confirmed by stepwise diffusion experiments with concentrations varying between successively higher sorbate concentration levels. All diffusion data reported herein refer to sorbate concentrations below 80% of equilibrium sorption. The ultimate sorption capacity of this sample of potassium T zeolite was 0.07–0.08 g hydrocarbon/g zeolite.

Results

Figure 5 shows the diffusion coefficient of *n*-paraffins in potassium T zeolite vs chain length at 300°C. It is seen that diffusivity decreases rapidly from ethane to propane, rises slightly at butane, then drops to a minimum at nC8. Above nC8, *diffusivity rises rapidly* to a maximum at about nC12, then decreases again. At 300°C, *the n-dodecane molecule is moving through the zeolite lattice at about 140 times the velocity of the n-octane molecule, despite the difference in size.* In fact, at 300°C, *n*-dodecane has a diffusiv-

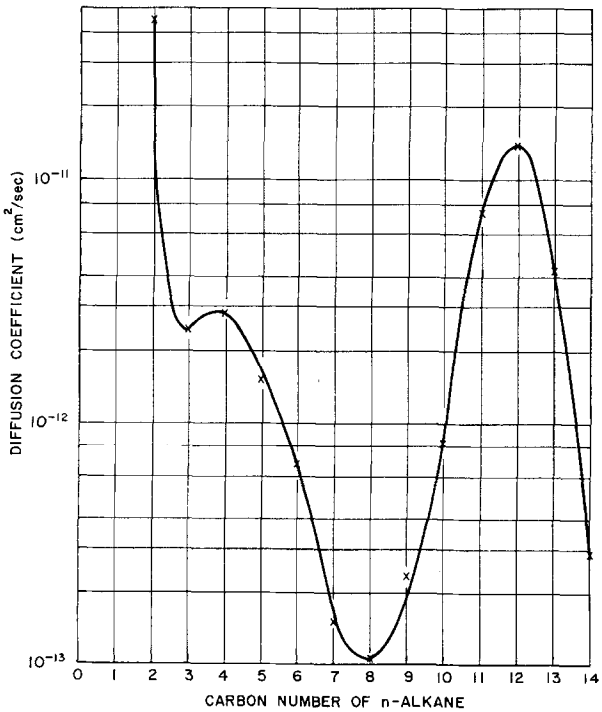

FIG. 5. Diffusion coefficients of *n*-alkanes in potassium T zeolite at 300°C.

ity six times greater than that of propane at the same temperature.

The high values of diffusion coefficients in the nC11–nC12 range relative to the much lower values at nC8 and nC14 indicate that the zeolite presents a "window of high transmittance" to molecules of a certain critical length but not to those either shorter or longer. This phenomenon will be designated as the "window effect."

Figures 6, 7, and 8 present Arrhenius plots of diffusion coefficients for ethane through tetradecane and some polar molecules. In most cases, experiments were continued either until the ultimate intrazeolitic concentration of 7–8% wt% sorbate was reached or until sorption had lined out at some lower equilibrium concentration, depending on the adsorption isotherm. Figures 6–8 show that diffusion of all C3–C13 n-paraffins is closely described by the Arrhenius relationship $D = D_0 \exp(-E/RT)$. This behavior, which yields temperature-independent diffusional activation energies, E, is seen to be maintained over very wide ranges—in the case of n-heptane over a 21,000-fold change in D (Fig. 6).

Diffusion of ethane (Fig. 6) differed from that of the higher paraffins in that activation energy was not constant and significant concentration dependence was observed above 50% of equilibrium. Ethane data in Fig. 6 are for sorbate concentrations below 50% of equilibrium. The 300°C ethane

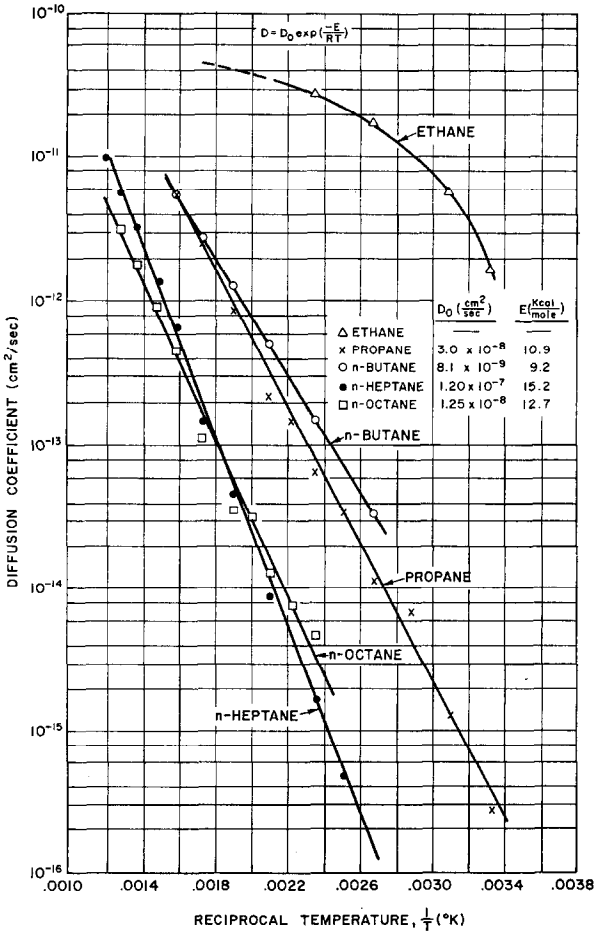

FIG. 6. Diffusion coefficients of hydrocarbons in potassium T zeolite.

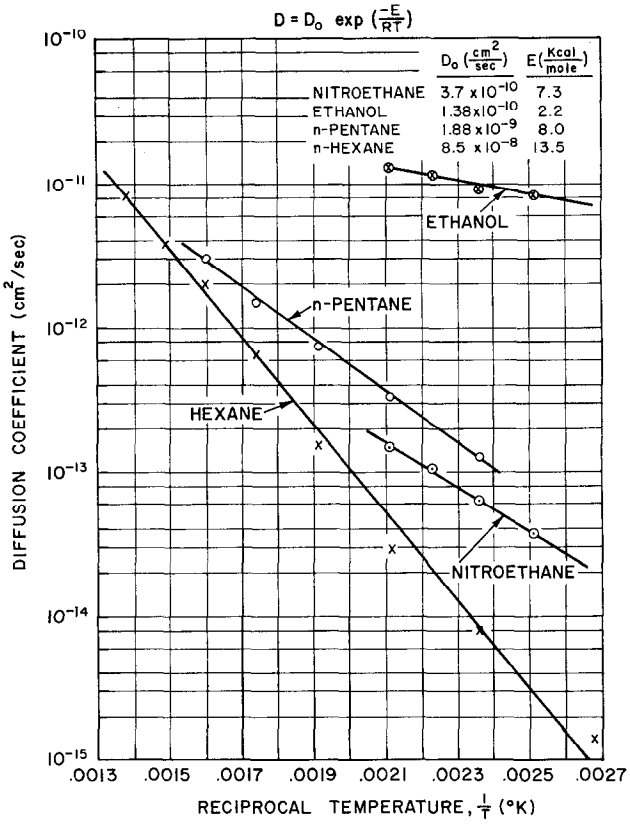

FIG. 7. Diffusion coefficients of hydrocarbons in potassium T zeolite.

point in Fig. 5 was estimated via the indicated extrapolation in Fig. 6.

The window effect is seen from Fig. 9 to persist over wide ranges of temperature. Although higher temperatures tend to decrease the depth of the window, the effect is still readily apparent at the catalytically interesting temperature of 450°C.

Figure 10 illustrates the large variation in pre-exponential (frequency) factors and activation energies encountered for the homologous series of *n*-paraffins. It is seen that the change of a few $-CH_2$ groups can vary the contribution of the frequency factor, D_0, and $\exp(-E/RT)$ by whole orders of magnitude. Figure 10 also demonstrates a clear-cut compensation effect in which the frequency factor, D_0, increases as the activation energy, E, increases.

The observed independence of diffusivity on intracrystalline sorbate concentration can be interpreted in terms of the physical model of this diffusion process. Reference to Figs. 1 and 2 shows that both the offretite large pore and the erionite large cavity are girthed by 12-membered oxygen rings. The free diameter of this 12-ring, clear inside the oxygen atoms, is 6.3 Å. The radius of a normal paraffin in the tetrahedrally staggered configuration is ~6.4 Å. The computed maximum clearance of 0.85 Å indicates a severely limited range of molecular spatial configurations within the zeolite lattice. Whatever the precise configuration, *n*-paraffins molecules are closely sheathed by the zeolite T cavity within which they are located—precluding direct side-to-side interactions. In zeolite T, *n*-paraffins can interact directly with each other in the following ways. These are the "end-to-end" positions assumed by molecules aligned in either the $\bar{a}$ or $\bar{c}$ direction (see Figs. 1–3), or the "end-

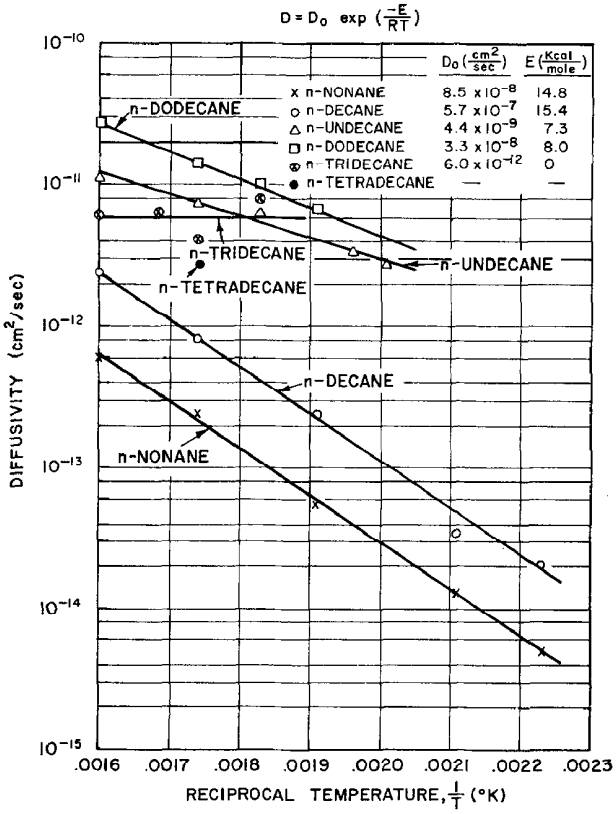

FIG. 8. Diffusion coefficients of hydrocarbons in potassium T zeolite.

to-side" positions assumed when two molecules aligned in different crystal directions contact each other through an 8-membered ring.

The foregoing considerations suggest a model in which hydrocarbon molecule–molecule interactions are likely to be weak and the most significant forces acting upon diffusing *n*-paraffins will be those arising from their interaction with the zeolite lattice and cations. The essence of this model is that diffusional energetics are controlled primarily by molecule–lattice interactions while molecule–molecule interactions contribute primarily via the statistics of place exchange (i.e., whether or not the target site for a migrating molecule is occupied or not). From the preceding, it is apparent that the intrazeolitic guest molecules constitute an interstitial occluded phase—as has also been discussed by Kington and Laing (*24*). The diffusion model envisioned in this study is termed "single-phase, single-site, unidirectional diffusion into an initially empty zeolite." For brevity, the coefficient is termed the "unidirectional diffusivity," and should be carefully distinguished from, for example, binary sorbate exchange or single-file diffusion constants, etc. (*7*).

As discussed in the Experimental section, diffusivities were observed to be concentration independent (below about 80% of saturation). The theoretical interpretation of the unidirectional diffusion process thus reduces to a simple, single parameter, Fickian framework.

DISCUSSION

From Fig. 5 it is clear that, with the window effect, we are dealing with a phenomenon which is unexpected when compared with conventional transport in large-pored catalysts—where diffusivities decrease

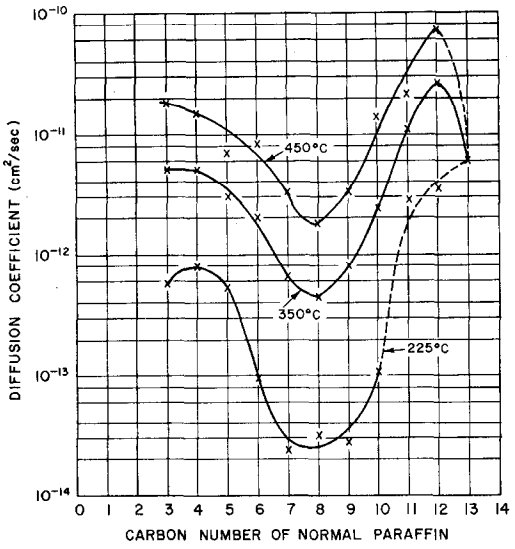

FIG. 9. Effect of temperature on window effect associated with diffusion of *n*-paraffins in potassium T zeolite.

monotonically with the square root of molecular weight and generally lie in the range 10^{-1}–10^{-5} cm²/sec. The periodic nature of the diffusivity/carbon number relation (Fig. 5) suggests seeking an interpretation in terms of the periodic nature of the zeolite lattice.

Window Effect

The window effect, as illustrated in Fig. 5, involves the diffusion coefficient reaching a minimum at *n*-octane, with the larger molecules, such as *n*-dodecane, having orders-of-magnitude greater mobility than *n*-octane. The interpretation for this phenomenon is summarized as follows: the length of *n*-octane corresponds almost exactly to the free length of the erionite cage defined by the aluminosilicate framework. The close sheathing of the *n*-octane molecule by the hexagonally shaped erionite cage yields a

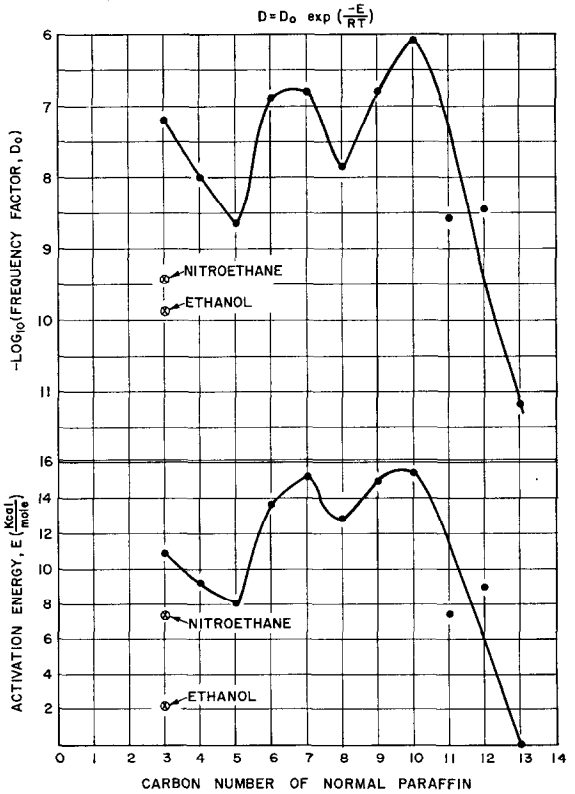

FIG. 10. Activation energy and frequency factor for *n*-paraffin diffusion in potassium T zeolite.

configuration where the molecule just fits the cavity. It is in a low-energy trap defined by the cage with the primary energy barrier to diffusion deriving from the 8-membered rings forming the cage's exit/entry ports. Entrapment in the cage leads to low mobility for "just-fitting" molecules such as nC7–8. Molecules larger than nC8 are too long to entirely fit into the erionite cage and must assume a configuration with part of the molecule extending through at least one 8-membered ring constituting the aluminosilicate framework. This extension through an 8-ring is conceived to result in a partial surmounting of the energy barrier by virtue of molecular size alone. Channelization of the *n*-paraffin through the 8-ring results in high selectivity to successful forward translation via both a lowered energy barrier and an imposed molecular orientation in the direction required for migration (entropic effect). Thus, larger molecules can have enhanced mobility as shown in Fig. 5.

A more detailed analysis of the window effect is as follows: From structural considerations (Fig. 1) the net, free interior dimensions of an erionite cage approximate a 13.0 × 6.3 Å cylinder. From Table 1, which summarizes *n*-paraffin chain lengths, it is clear that the *n*-octane molecule (12.82 × 4.6 Å) will just "fill" an erionite cage and that only a single *n*-octane molecule can be accommodated. Focusing attention on the crystal $\bar{c}$ direction, we note that all molecules larger than *n*-octane will not be capable of aligning themselves entirely within a single large cavity in the $\bar{c}$ direction because of their size. For example, *n*-nonane is 14.1 Å long, but the large erionite cage is 13.0 Å in free length.

TABLE 1
LENGTH OF *n*-PARAFFINS

n-Paraffin	Length (Å)
C1	4.00
2	5.26
3	6.52
4	7.78
5	9.04
6	10.30
7	11.56
8	12.82
9	14.08
10	15.34
11	16.60
12	17.86
13	19.12
14	20.38

The crystal dimension of erionite in the $\bar{a}$ direction is 13.31 Å (Fig. 1). For an *n*-paraffin to clearly extend through a unit cell in the $\bar{a}$ direction, its net length must be the 13.3 Å center-to-center cell length plus about twice the oxygen atomic radius to account for the protrusion of the oxygens of the eight-membered rings. This is 13.3 + (2)(1.4) = 16.1 Å. The net length of an *n*-alkane oriented in the $\bar{a}$ lattice direction is its normal length (given by Table 1) multiplied by cosine 30°—yielding a net length of 17.86 (cosine 30°) = 15.5 Å for *n*-dodecane. (The eight-membered rings in both erionite and offretite are oriented ~30° to the plane perpendicular to the $\bar{a}$ direction. Overall length of *n*-paraffins, when aligned in the $\bar{a}$ direction, is reduced by cosine 30° due to their assuming a serpentine pattern through these rings.) This means that *n*-dodecane will just extend through the bounding eight-membered rings of a unit cell in the $\bar{a}$ direction—calculated above to be separated by 16.1 Å. Molecules smaller than this will not be able to extend through this unit cell and will be in contact with only two eight-membered rings instead of three.

With these facts in mind, we are now in a position to propose some detailed interpretations of the window effect seen in Fig. 5. Molecules from propane to *n*-octane are small enough to orient themselves with axes in the $\bar{c}$ direction in the large erionite cavities (free height 13.0 Å). In this configuration, the molecule has the capability to be aligned in the lattice orientation which has the lowest diffusivity ($\bar{c}$ direction). It also can be entirely located in a deep potential well relative to *n*-nonane and larger which are too long to fit in the large cage and which must extend through eight-membered rings. Therefore, a smooth decrease in diffusivity, due to molecular weight effects,

is expected between C3 and C8. Figure 5 shows that this is the case.

When *n*-nonane is considered, however, the steric factor comes into prominence. The large cage is 13.0 Å in length, but n-C9 is 14.1 Å long. Thus, n-C9 and longer molecules can exist in the structure only by extending through an eight-membered ring and by orienting themselves partially or wholly in the $\bar{a}$ direction. Since this is considered the direction of highest diffusivity, n-C9 and longer chains might be expected to exhibit a higher diffusivity than n-C8. Figure 5 shows that this is the case. The steadily rising diffusivity from n-C9 to n-C12 may be a consequence of the increasingly greater fraction of the longer molecule's chain length which orients in the $\bar{a}$ direction in order to fit into the lattice without being capable of becoming entirely trapped in deep potential wells.

As discussed previously, n-C12 is the shortest molecule that can extend entirely through a unit cell in the $\bar{a}$ direction. At this point it just extends to the extremes of the two eight-membered rings defining the extremes of the unit cell in the $\bar{a}$ direction and is just supported by three eight-membered rings. From this, we might infer that the dimension of the n-C12 molecule is a critical point on the curve. Figure 5 shows that this is the case.

Molecules larger than C12 can easily bridge the $\bar{a}$ direction unit cell gap and will, therefore, encounter a fairly well "averaged" potential energy distribution in the lattice. For molecules C12 and larger, then, simple molecular weight and steric interference effects can be expected to take over. Diffusivity will then decrease in the range C12–C14 and Fig. 5 shows this.

The previous structural interpretations of the window effect (Fig. 5) are qualitatively supported by the activation energies shown in Fig. 10. The decrease of activation energy from 15.3 kcal for C10 to about 8 kcal for C11–C12 coincides with the potential ability of these larger molecules to nearly bridge the gap between the extreme dimensions of the erionite or offretite unit cell in the $\bar{a}$ direction. n-C12 can almost extend to the ultimate extremes of the eight-membered rings bounding the unit cell in the $\bar{a}$ direction and was shown to have the greatest diffusivity of all the large *n*-paraffins. Figure 5 indicates n-C11 to have a diffusivity nearly as great as n-C12. This suggests that the bridging of the $\bar{a}$ direction unit cell begins to a certain degree with n-C11. The decrease in activation energy to 8 kcal for n-C11 and n-C12 is seen to coincide with this ability to bridge three eight-membered rings and thus remain partly out of the potential well. The activation energy indicates that these molecules still interact sufficiently with the potential field to require 8 kcal for migration. This is reasonable in view of the fact that an n-C12 molecule will sometimes be in the "just bridged" position and sometimes in an intermediate position with its extremes somewhere between 8-membered rings.

The activation energy for n-C13 is approximately zero. Here the molecule appears to be able to bridge over a sufficient number of rings in the $\bar{a}$ direction in that it "ignores" the potential gradients in the zeolite lattice.

A clue to the sudden increase in activation energy between n-C5 and n-C6 (Fig. 10) may be found in the relative sizes of the molecules and the large cavity of erionite. The large erionite cavity is oriented in the $\bar{c}$ crystallographic direction and is 13.0 Å in free length when the size of the oxygen atoms in the bounding planar 6-membered rings is accounted for. Figure 2(b) shows that the minimum dimension of the 8-membered ring is 3.6 A. This is the dimension which controls the diffusive process. Now, picture an *n*-pentane molecule oriented in the $\bar{c}$ direction with one-CH_3 group as close as possible to the planar 6-membered ring A [Fig. 2(a)]. This molecule will completely block off the 8-membered rings in the lower half of the large cavity and leave a clearance in the $\bar{a}$ direction of 3.96 Å in the 8-rings in the upper half. (Net clearance is height of cell minus length of *n*-pentane = 13.0 − 9.04 = 3.96 Å.) Referring to Fig. 2(b), it is seen that a n-C5 molecule in the lower part of the large cage closes the upper 8-rings to the dimensions of (approximately) 3.96 × 3.6 × 3.7 Å. Since we have already seen that molecules will pass the 3.6 Å dimension, it is felt that closing the 5.2 Å dimen-

sion to 3.96 Å will not be of first-order influence on the activation energy.

Thus, an *n*-pentane molecule located in the lower half of the large cavity [Fig. 2(a)] is not expected to seriously obstruct a molecule diffusing in the $\bar{a}$ direction [path (a) in Fig. 2(a)] through the upper half. However, for *n*-hexane and larger, a single molecule aligned in the $\bar{c}$ direction in the erionite cage will obstruct diffusion of other molecules in the $\bar{a}$ direction. This increased obstruction to diffusion in the $\bar{a}$ direction may be the source of the large jump in activation energy and frequency factor between n-C5 and n-C6 (Fig. 10). It may be termed "stacking interference."

Figures 7 and 10 summarize some results for ethanol and nitroethane—which may be considered as analogs of propane with a terminal $-CH_3$ replaced by polar functional groups. It is noteworthy that ethanol has a diffusivity about 150 times that of propane. The large-scale shifts in frequency factors and activation energies shown in Fig. 10 suggest that the permanent dipoles of ethanol and nitroethane play an essential role in the diffusion mechanism.

Implications for Shape-Selective Catalysis

Figure 11(a) shows the product distribution from the catalytic cracking of n-C23 over H-erionite at 340°C as reported by Chen, Lucki, and Mower (*5*). Note the maxima in products at C3–4 and C11–12. Figure 11(b) shows the diffusivity of the *n*-paraffins in potassium T zeolite, also at 340°C, vs carbon number from Figs. 6–8. Diffusion maxima at C3–4 and C11–12 are also observed—paralleling the product maxima. The virtual absence of n-C7–9 in the cracked products has its counterpart in the *diffusion minimum* at the same carbon numbers. As shown in Fig. 2 of (*5*), cracking of long-chain paraffins over large-pored zeolites or silica-alumina yields a smooth product distribution, having a *maximum*

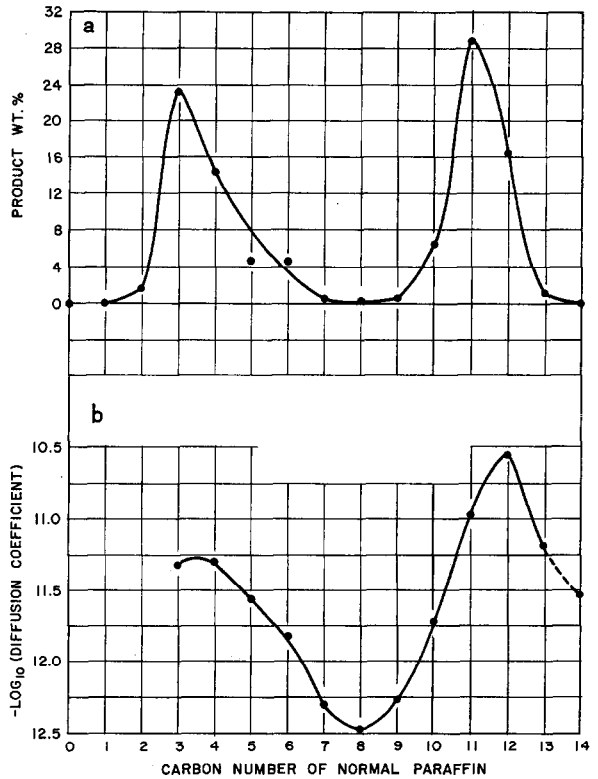

FIG. 11. (a) Product distribution from cracking *n*-tricosane over H-erionite at 340°C [Ref. (*5*)]. (b) Diffusion coefficient of *n*-paraffins in potassium T zeolite at 340°C.

yield in the range C6–C9. Therefore, the bimodal yield pattern for cracking over erionite [Fig. 11(a)] is unexpected on the basis of classical cracking mechanisms.

The manner in which the diffusion window effect results in the bimodal product distribution of Fig. 11(a) is interpreted as follows: Long paraffins are initially cracked to the expected primary product distribution composed of a wide range of carbon numbers. However, C7–C9, having a very low diffusivity (relative to C3–4 and C11–12) (Figs. 5 and 11), are effectively trapped in the zeolite until they crack to C3–C4 molecules. These can then emanate from the erionite or T crystal by virtue of their much higher diffusion rates. The product maximum at C11–12 [Fig. 11(a)] occurs when a product molecule of this size is formed and then can quickly diffuse out of the erionite/T crystal before being cracked.

Miale, Chen and Weisz (*3*) computed an upper limit to the diffusivity of *n*-hexane in H-erionite of 10^{-9} cm²/sec on the basis of cracking rate data in the temperature range 390–430°C. This is consistent with the actually measured value of $\sim 5 \times 10^{-12}$ cm²/sec (Fig. 7) for KT zeolite—even allowing an order of magnitude for the difference in cation size. These authors (*3*) measured an activation energy of 18 kcal/mole for diffusion-controlled n-C6 cracking on H-erionite and ~28.5 kcal/mole for cracking under non diffusion-controlled conditions. Note from Fig. 7 that E_D for n-C6 diffusion is 13.5 kcal/mole and that the apparent activation energy for a reaction controlled by activated diffusion is $(E_R + E_D)/2$ (where E_R and E_D are the activation energies for reaction and diffusion, respectively). The apparent activation energy for n-C6 cracking is then calculated to be $(28.5 + 13.5)/2 = 21$ kcal/mole comparing well with the observed (*3*) value of 18 kcal/mole.

Summary and Conclusions

Diffusion of *n*-paraffins in zeolite T exhibits the unusual effect that *n*-octane molecules migrate much more slowly than either *n*-butane or *n*-dodecane. This window effect is related to the close fit between molecule and zeolite pore and the strongly orienting influence of the lattice structure on sorbed molecules. Maxima and minima in diffusion coefficients appear to be clearly related to known crystal dimensions. Occurrence of the window effect is thought to be a general phenomenon, common to diffusion of long molecules in many zeolites, with the position of minima/maxima determined by identifiable crystal parameters. Extension of diffusion measurements to longer paraffins, polar molecules and other zeolites, such as chabazite, levynite, gmelinite, etc. is indicated.

Occurrence of the compensation effect suggests a concerted action in which entropic factors (orientation) are correlated with energetic factors (jumping through 8-membered rings). The periodic nature of the diffusivity (Fig. 5) suggests that the oscillatory, configurational motion of both vibrating lattice and *n*-alkane may also play a significant role as suggested recently by Weisz (*25*).

As shown by Riekert (*7*), the individual species diffusivities for binary sorption, single-file diffusion, etc. are obtained by a combination of D, statistical factors involving site occupancy, and phase boundary dynamics. Thus, the unidirectional diffusivity, D, is a basic quantity directly applicable to more complex processes in zeolites, in particular to steady state catalytic observations.

The principal result of this study is the observation that large molecules can diffuse hundreds of times faster than smaller ones in shape-selective zeolite KT. As a result of this effect, catalytic product distributions can be unexpectedly shifted by superposition of structure-sensitive mobility variations on the primary reaction pattern.

Acknowledgments

The author wishes to thank Drs. P. B. Weisz, N. Y. Chen, and C. D. Prater for very valuable suggestions and discussions.

References

1. Weisz, P. B., and Frilette, V. J., *J. Phys. Chem.* **64**, 382 (1960).
2. Weisz, P. B., Frilette, V. J., Maatman, R. W., and Mower, E. B., *J. Catal.* **1**, 307 (1962).
3. Miale, J. N., Chen, N. Y., and Weisz, P. B., *J. Catal.* **6**, 278 (1966).

4. CHEN, N. Y., AND WEISZ, P. B., *Chem. Eng. Progr., Symp. Ser.* **67**, No. 73, 86 (1967).
5. CHEN, N. Y., LUCKI, S. J., AND MOWER, E. B., *J. Catal.* **13**, 329 (1969).
6. CHEN, N. Y., "Proc. 5th Int'l. Congr. Catalysis," Paper 100, West Palm Beach, U. S. A., 1972.
7. RIEKERT, L., *Advan. Catal.* **21**, 281 (1970).
8. BARRER, R. M., *Advan. Chem.* **102**, 1 (1971).
9. RIEKERT, L., *AIChE J.* **17**, 446 (1971).
10. RIEKERT, L., "4th Int'l. Congr. Catalysis," Paper 18, Symposium III, Moscow, U.S.S.R., 1968.
11. BARRER, R. M., AND KERR, I. S., *Trans. Faraday Soc.* **55**, 1915 (1959).
12. EBERLY, P. E., JR., *Amer. Mineralogist* **49**, 30 (1964).
13. EBERLY, P. E., JR., *Ind. Eng. Chem., Prod. Res. Dev.* **8**, 140 (1969).
14. BARRER, R. M., AND IBBITSON, D. A., *Trans. Faraday Soc.* **40**, 206 (1944).
15. BENNETT, J. M., AND GARD, J. A., *Nature (London)* **214**, 1005 (1967).
16. GARD, J. A., AND TAIT, J. M., *Advan. Chem.* **101**, 230 (1971).
17. WHYTE, T. E., JR., WU, E. L., KERR, G. T., AND VENUTO, P. B., *J. Catal.* **20**, 88 (1971).
18. WU, E. L., WHYTE, T. E., JR., AND VENUTO, P. B., *J. Catal.* **21**, 384 (1971).
19. AIELLO, R., BARRER, R. M., DAVIES, J. A., AND KERR, I. S., *Trans. Faraday Soc.* **66**, 1610 (1970).
20. KOKOTAILO, G. T., SAWRUK, S., AND LAWTON, S. L., *Amer. Mineralogist* **57**, 439 (1972).
21. BRECK, D. W., AND ACARA, N. A., U. S. Patent 2,950,952, August 30 (1960).
22. SHERRY, H. S., Proc. Int'l. Congr. "Ion Exchange in the Process Industries," p. 329, July 16–18, 1969, Soc. Chem. Ind., London, 1970.
23. CRANK, J., *in* "The Mathematics of Diffusion," pp. 62–72, Oxford, Clarendon Press, London, 1956.
24. KINGTON, G. L., AND LAING, W., *Trans. Faraday Soc.* **51**, 287 (1955).
25. WEISZ, P. B., *Chem. Tech.*, to be published.